scientific reports

Check for updates

OPEN

Nanoplastics impair antitumor NK and CD8+ T cell cytotoxicity and antiviral B cell antibody responses to SARS-CoV-2

Stefano Maria Santini[1], Francesca Spadaro[2], Agostina Pietrantoni[2], Irene Canini[1], Simona Donati[1], Barbara De Berardis[3], Caterina Lapenta[1], Alessandra Fragale[1], Laura Lattanzi[1], Giulia Romagnoli[1], Stefania Rossi[1], Sara Gualdi[1], Maria Carollo[2], Federica Frasca[4], Carolina Scagnolari[4] & Lucia Gabriele[1]✉

Nanoplastics are pervasive environmental contaminants that continuously expose humans and accumulate in multiple organs. Increasing evidence associates NPs with adverse health effects, including inflammation and carcinogenesis, yet their impact on human innate and adaptive immunity remains poorly understood. This knowledge gap is particularly relevant for diseases treated with therapies that modulate immune responses. Here, we investigated the effects of NP exposure on major subsets of human peripheral lymphocytes, essential for antitumor and antiviral defense while preserving immune tolerance. Peripheral blood mononuclear cells from healthy donors were exposed to oxidized and plasma-exposed NPs, which acquired a stable protein corona. NP exposure induced a time-dependent increase in immune cell interactions and resulted in reduced activation and functionality of CD4+ and CD8+ T cells, B cells, and natural killer cells. T lymphocytes displayed impaired tumor antigen-specific responses, while natural killer cells showed decreased tumor cell-killing capacity. Notably, B cells internalized NPs, leading to reduced ability to generate antibodies against SARS-CoV-2. Overall, these findings demonstrate that NPs compromise both innate and adaptive immune functions, weakening antiviral and antitumor responses. Our results highlight potential risks associated with NP exposure for susceptibility to infections and cancer as well as immune-based therapy efficacy.

Keywords Nanoplastics, Human immunity, Immune cell populations, Antitumor response, Antiviral response

Nanoplastics (NPs) have been detected worldwide and has captured scientific attention for their potential health effects. Microplastics (MPs) and NPs, < 100 nm in size, are generated from the breakdown of larger plastic debris, such as industrial abrasives, via processes like mechanical wear, weathering, photodegradation, hydrolysis, heat, and biological fragmentation[1]. NPs have a greater impact on health compared to MPs due to their smaller size, which allows them to easily cross biological membranes and enter endocytosis pathways. This enables them to accumulate in organs and contribute to long-term damage in systems such as the respiratory, gastrointestinal, cardiovascular, hepatic, renal, reproductive systems[2]. Importantly, long-term environmental exposure to NPs may impact and exacerbate inflammation affecting the outcome and therapeutic response of non-communicable diseases, such as cancer[3]. Environmental aging alters the physicochemical properties of NPs, thereby influencing protein corona composition in bodily fluids such as blood and ultimately affecting their adsorption patterns to cells; thus, this process plays a critical role in determining the biological activity of NPs within the human body[4]. Measurable levels of NPs were found in the blood of human volunteers[5–7]. These findings raise concerns about the effect of NPs on immune cells, which are a key component of blood. Notably, while various studies have emphasized the effects of NPs on the immune system, most of this research has focused on murine models and

[1]Department of Oncology and Molecular Medicine, Istituto Superiore di Sanità, 00161 Rome, Italy. [2]Core Facilities Technical-Scientific Service, Istituto Superiore di Sanità, Rome 00161, Italy. [3]Artificial Intelligence and Innovative Technologies for Health, Istituto Superiore di Sanità, Rome 00161, Italy. [4]Department of Molecular Medicine, Laboratory of Virology, Sapienza University of Rome, Rome, Italy. ✉email: lucia.gabriele@iss.it

cell lines, with only a limited number examining human primary cells. Moreover, no reports have yet explored the functionality of key immune populations that regulate both innate and adaptive immune responses[2].

Polystyrene NPs are widespread environmental polymers that, upon human exposure, can disrupt the blood-brain barrier, damage endothelial cells, and promote colitis-associated cancer through lipid metabolism disruption and DNA damage[8,9]. From an immunological perspective, in vivo and in vitro studies demonstrate that NPs can interfere with immune cell populations, including macrophages, dendritic cells (DCs), neutrophils, T cells, B cells, and natural killer (NK) cells[10]. In mice, prolonged exposure to NPs leads to increased intestinal permeability and disruption of the immune barrier, resulting in inflammation, a reduction in CD4 + and CD8 + T cells, and dysregulation of B cells[11]. Human peripheral blood lymphocytes (PBLs) have been reported as targets of the genotoxic and cytotoxic effects of NPs[12]. In terms of immune response, T and B lymphocytes are key players in adaptive immunity, with B cells determining antibody specificity and CD8 + T cells targeting infected or cancerous cells. CD4 + T helper (Th) cells produce cytokines to support immune activity, while NK cells eliminate infected or tumor cells without prior exposure. Human lymphocytes have been reported to take up NPs, albeit at a much lower rate, than cells of the monocyte-macrophage lineage, which are the primary cells involved in the uptake and internalization of NPs[13,14]. CD4 + Th and cytotoxic CD8 + T cells showed reduced viability and downregulation of activation markers after 24 h of exposure to 70 nm NPs, along with modulation of key cytokines like IL-1β, IFN-γ, IL-6, TNFα and IL-17A[15]. The suppressive effects of 50 nm NPs were also observed in murine splenic lymphocytes, characterized by low particle uptake, apoptosis, oxidative stress, and inhibited T cell activation. This was evident from the downregulation of CD25 + and CD69 + markers, reduced IL-2 and IFN-γ production, and decreased phospho-IκBα, phospho-IKKβ, and phospho-STAT5 activation[16]. A study using the Raji-B cellular model, representative of B lymphocytes, demonstrated low NP uptake along with mild toxicity, reactive oxygen species (ROS) production, and genotoxicity[17]. Moreover, NK cells were identified as an immune population affected by MP exposure, playing a key role in liver inflammation in mice chronically exposed[18,19]. Nevertheless, a direct link between phenotypic and functional immune modulation of human lymphocytes following NP exposure has not yet been established.

In this study, we focused on the lymphocyte component of human peripheral blood and conducted a comprehensive analysis of the effects of NPs on key lymphocyte subsets essential for effective immune responses. Our findings demonstrate that NPs rapidly acquire a protein corona upon exposure to plasma, which mediates significant interactions with major lymphocyte subsets leading to the downregulation of immune responses at both phenotypic and functional levels. Notably, we found that the immunosuppressive environment induced by NPs severely affects the functional response of critical immune subsets, such as CD8 + T lymphocytes and NK cells, thereby impairing antigen-specific immune response against cancer cells. In addition, NPs were found to inhibit IgG production in activated B cells in response to SARS-Co-V2 infection.

Results

NP functionalization

To mimic aged environmental NPs with diverse sizes and chemical modifications, we conducted our experiments using functionalized polystyrene NPs[20]. Commercially available original (or)-NPs were thermally treated at 80 °C to induce oxidation, allowing the presence of carboxyl, alkoxyl and hydroxyl groups on the particle surface. Oxidized (ox)-NPs were then incubated with plasma from the same donor from whom PBMC were isolated to form a donor-specific protein corona while retaining colloidal stability, thereby reproducing the natural biological coating present in the blood and yielding plasma-coated ox-NPs (Pl-ox-NPs; also referred to as NPs). Transmission electron microscopy (TEM) analysis showed that or-NPs resuspended in PBS, were well dispersed and not agglomerated (Fig. 1A). Following oxidation, NPs agglomerated, forming clusters with diameters up to ~ 1.5 µm (Fig. 1B). Notably, large NPs agglomerates surrounded by a protein corona were observed after 2 h-incubation with plasma (Fig. 1C). Evidence for protein corona formation was provided by the significant differential enlargement in the average diameters of Pl-ox-NPs relative to or-NPs and untreated ox-NPs (Fig. 1D). These findings were complemented by dynamic light scattering (DLS) measurements, which provided hydrodynamic diameter (Z-average), polydispersity index (PDI) and surface charge (zeta potential) values for all NP groups (Fig. 1; Table 1). The or-NPs exhibited a PDI close to 0.1, consistent with a monodisperse suspension and their size distribution displayed a single, narrow peak centred around 126 nm (Fig. 1E). In contrast, ox-NPs showed significantly increased hydrodynamic diameters and PDI values, indicative of polydispersity and particle agglomeration. Intensity-based size distributions revealed a dominant peak at 1.9 µm and a minor peak near 170 nm (Fig. 1E), while the high Z-average value likely arose from the dependence of scattering intensity on particles with the sixth power of radius, causing signals from large agglomerates to dominate over smaller particles. When suspended in plasma for 2 h, Pl-ox-NPs showed agglomeration, with three main populations observed (~ 5.4 µm, 267 nm, and 44 nm, the latter likely corresponding to protein aggregates), and the high polydispersity (PDI > 0.7) precluded a reliable Z-average measurement (Fig. 1E; Table 1). Due to the high polydispersity (PDI > 0.7), a reliable Z-average could not be determined for these particles (Fig. 1; Table 1). Importantly, these features were maintained for up to 48 h of plasma incubation (Fig. S1). Zeta potential measurements showed that or-NPs were negatively charged in PBS, while oxidation reduced their negative surface charge, indicating decreased suspension stability consistent with the increased PDI values. Pl-ox-NPs showed even greater instability, with zeta potential shifting toward less negative values, reflecting protein adsorption and corona formation that promoted agglomeration, as confirmed by DLS analysis. Notably, all the characteristics exhibited by NPs upon plasma exposure were confirmed and recapitulated by incubating ox-NPs with human serum (Fig. S2).

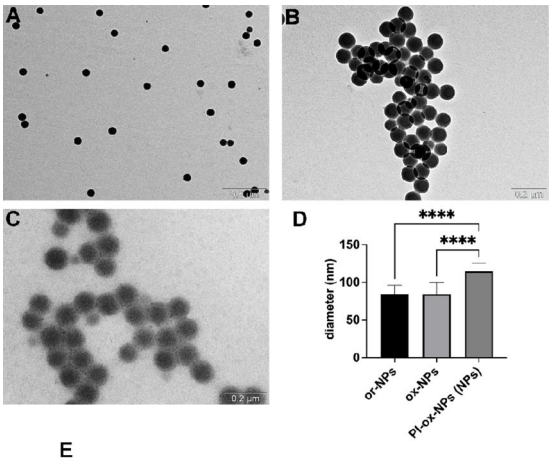

Table 1

Sample	Z-Average (nm)	PDI	Zeta potential (mV)
or-NPs	123,0 ±0,6	0,149 ± 0,009	-19,0 ± 1,04
ox-NPs	2143 ± 160	0,435 ± 0,085	-11,3 ± 1,88
Pl-ox-NPs (NPs)	238,0 ± 3,5	0,832 ± 0,072	-7,08 ± 0,80

Fig. 1. Measurements of NPs. TEM of or-NPs in PBS (**A**), ox-NP in PBS (**B**), Pl-ox-NP exposed to Pl for 2 h (**C**). Graph showing the average diameters of NPs (**D**). Size distribution of or-NPs and ox-NPs in PBS and Pl-ox-NPs by DLS analysis (**E**). Hydrodynamic diameter (Z-Average), PDI and Zeta potential of or-NPs, ox-NPs and Pl-ox-NP (Table 1); $^{****}p \leq 0.0001$.

NPs enhance interactions between peripheral blood lymphocytes but lead to a less activated state

Human peripheral blood lymphocytes show low NP uptake, but the effects on their phenotype and function remain unknown[13]. We assessed the effects of Pl-ox-NPs (hereafter referred to as NPs) on PBMC proliferation and cell death, observing a slight, non-significant increase in proliferation and a higher live/dead ratio at 72 h versus controls (Fig. S3A, B). Further analysis of lymphocyte subset viability ($CD4^+$ and $CD8^+$ T cells, NK cells, B cells) up to 96 h post-NP exposure showed enhanced survival in all subsets except $CD8^+$ T cells. With IL-2, live $CD4^+$ and $CD8^+$ T cells were reduced at 72 h in NP-exposed cultures, while B cells and NK cells remained more viable at all time points (Fig. S3C-D). Next, we assessed the effects of NP exposure on the phenotype and function of individual lymphocyte subsets. NP-exposed $CD4^+$ T cells showed enhanced homotypic and heterotypic interactions, increasing cell conjugate formation up to 96 h (Fig. 2A-B). With IL-2, interactions were higher initially but declined by 96 h, unlike unexposed cells, which continued to increase (Fig. 2C). In addition, NP-exposed $CD4^+$ T cells cultured with IL-2 exhibited increased cytoplasmic granularity and cell size at 72 h, indicating altered cellular processes and limited NP uptake (Fig. 2D). TEM analysis showed that only a small fraction of $CD4^+$ T cells contained vacuoles with electron-dense NP-like material (Fig. 2E, Fig. S4). Flow cytometry revealed that NP exposure significantly downregulated activation markers (CD69, CD25, CD154, HLA-DR, CD38) and the inhibitory marker PD-1, broadly impairing T cell activation even in the presence of IL-2 (Fig. 2F, Fig. S5).

IL-2 (Fig. 4E-G). NP exposure also increased B cell interactions at 72 h, which then declined to levels similar to unexposed cells, a pattern also observed with IL-2 (Fig. 5A, C). NP-exposed B cells enlarged and developed intracellular granules, changes amplified by IL-2, with larger cells, abundant cytoplasm, and vacuoles containing NP-like material (Fig. 5B, D, E). Over time, TEM analysis showed few NP-containing vacuoles at 48 h, increasing substantially by 96 h (Fig. S6).

NPs attenuate immune activation and induce immunoregulatory markers

We next examined in depth the lymphocyte microenvironment shaped by NP exposure. Scanning Electron Microscopy (SEM) analysis showed that NP exposure enhanced $CD4^+$-$CD19^+$ cell conjugates, evident at 48 h, peaking at 72 h, and remaining prominent at 96 h (Fig. 6A, Fig. S6). These results indicate that changes in the immune environment are also driven by interactions among multiple lymphocyte populations. To

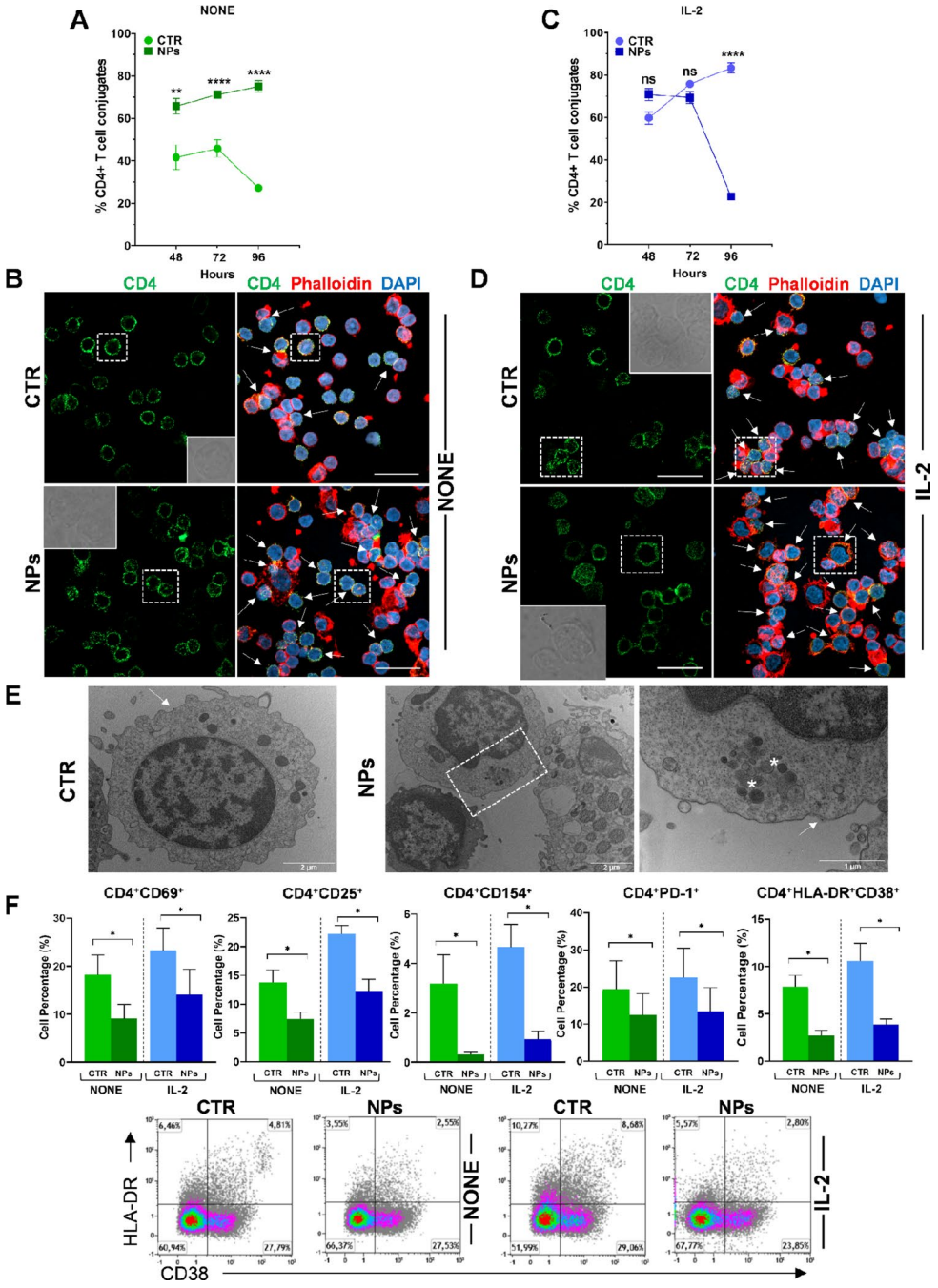

Fig. 2. NP effects on CD4 + T lymphocytes. (**A**, **C**) Time-course of CD4⁺ T cell interactions in PBMCs from CTR (A) or IL-2-stimulated (C) cultures exposed or not to NPs (48–96 h). Data represent mean % CD4⁺ cell conjugates ± SE; $^{**}p \leq 0.01$, $^{****}p \leq 0.0001$, ns: not significant. (**B**, **D**) Representative CLSM images of CD4⁺ T cells after 72 h NP exposure, stained for CD4 (green), actin (red), and nuclei (blue). White arrows indicate interacting cells; insets show transmission light images at higher magnification of Region Of Interest (ROI; dotted lines) with large vesicles in mainly in IL-2-stimulated NP-exposed cells. Scale bars= 20 µm. (**E**) TEM of CD4⁺ T cells ± NPs for 72 h, showing vacuoles with electrodense NP-like material (*). White arrows indicate anti-CD4 immunogold labeling; right panel shows magnified ROI. (**F**) Flow cytometry of activation markers in CD3⁺CD4⁺ T cells after 72 h-NP exposure (mean ± SE; $^{*}p \leq 0.05$). Data are representative of three independent experiments. Similarly, NP-exposed CD8⁺ T cells showed increased cell interactions over time, peaking at 96 h and forming clusters of highly granular cells by 72 h (Fig. 3A-B). With IL-2, NP exposure did not alter interaction rates, and cell conjugates declined at 96 h, yet clustering with densely granular cytoplasm was consistently observed (Fig. 3C-D). NP exposure also significantly downregulated early-activated CD69⁺CD8⁺ T cells, activated CD25⁺CD8⁺ cells, and highly activated HLA-DR⁺CD38⁺CD8⁺ subsets, with a trend toward PD-1 downregulation, though not statistically significant (Fig. 3E).

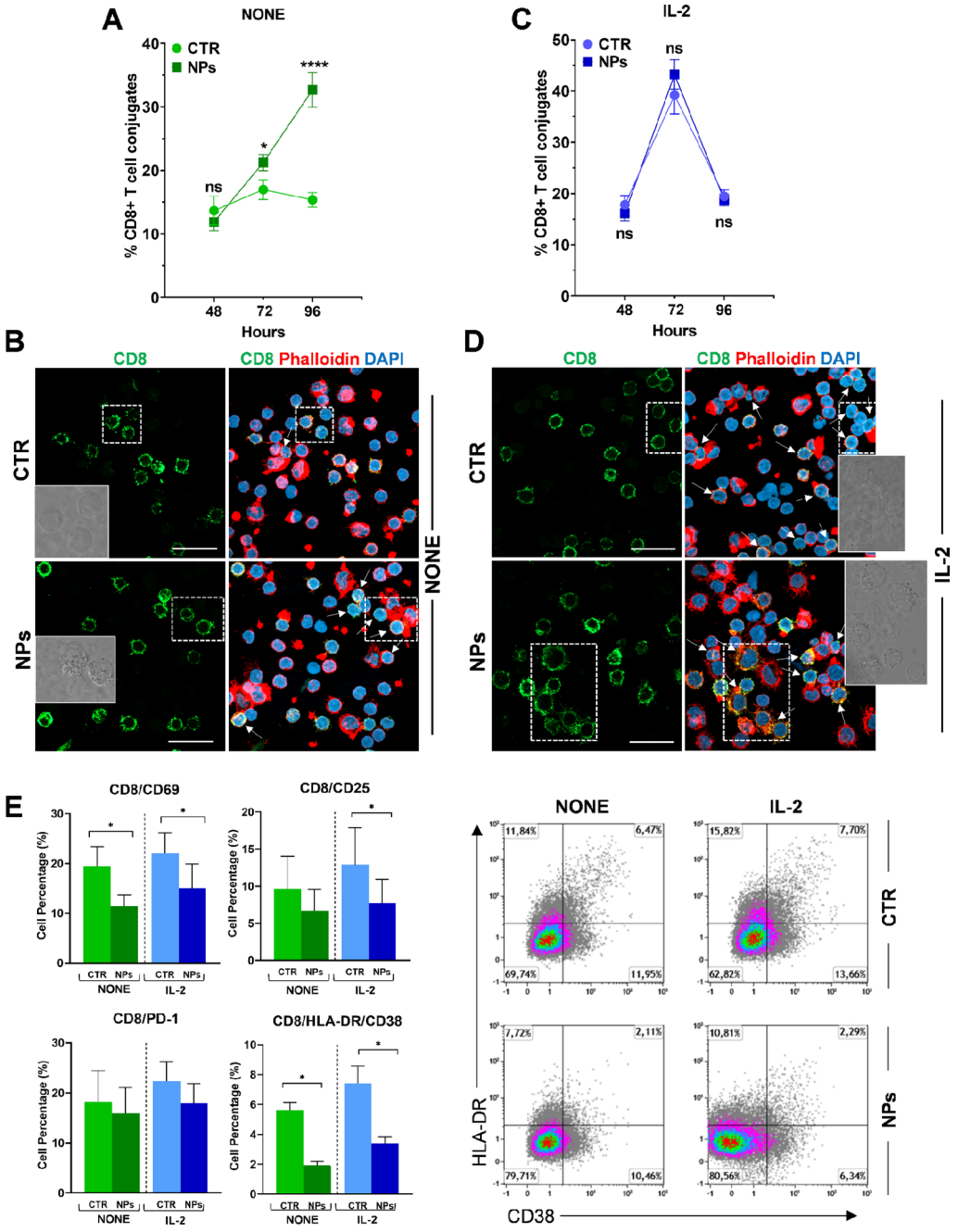

Fig. 3. Impact of NPs on CD8 + T lymphocytes. (**A**, **C**) Time-course of CD8⁺ T cell interactions in PBMCs from CTR (A) or IL-2-stimulated (C) cultures exposed or not to NPs for 48–96 h. Data show mean % CD8⁺ cell conjugates ± SE; $*p \leq 0.05$, $****p \leq 0.0001$. (**B**, **D**) CLSM images of CD8⁺ T cells after 72 h-NP exposure, stained for CD8 (green), actin (red), and nuclei (blue). White arrows indicate interacting cells, with a higher frequency of in NP-exposed cells; insets show transmission light images of higher magnification of ROI (dotted lines) with vesicle-containing cells mainly in IL-2-stimulated NP-exposed cultures. Scale bars=20 µm. (**E**) Flow cytometry of CD8⁺ T cells after 96 h NP exposure, showing activation markers (HLA-DR, CD38) in CTR or IL-2 conditions of three independent experiments (mean ± SE; $*p \leq 0.05$); left panel: representative flow cytometry plots.Analysis of NK cells also revealed enhanced interactions in the presence of NPs, peaking at 96 h (Fig. 4A). (Fig. 4A). Unlike T cells, NP exposure enhanced CD56⁺ cell conjugates even with IL-2, without decline at later time points (Fig. 4C). CSLM revealed limited effects on NK cell granularity compared to CD4⁺ and CD8⁺ lymphocytes (Fig. 4B, D). However, NP exposure impaired NK function, reducing CD107a⁺ and IFN-γ⁺ cells after K562 co-culture and decreasing cytotoxicity, both with and without IL-2.

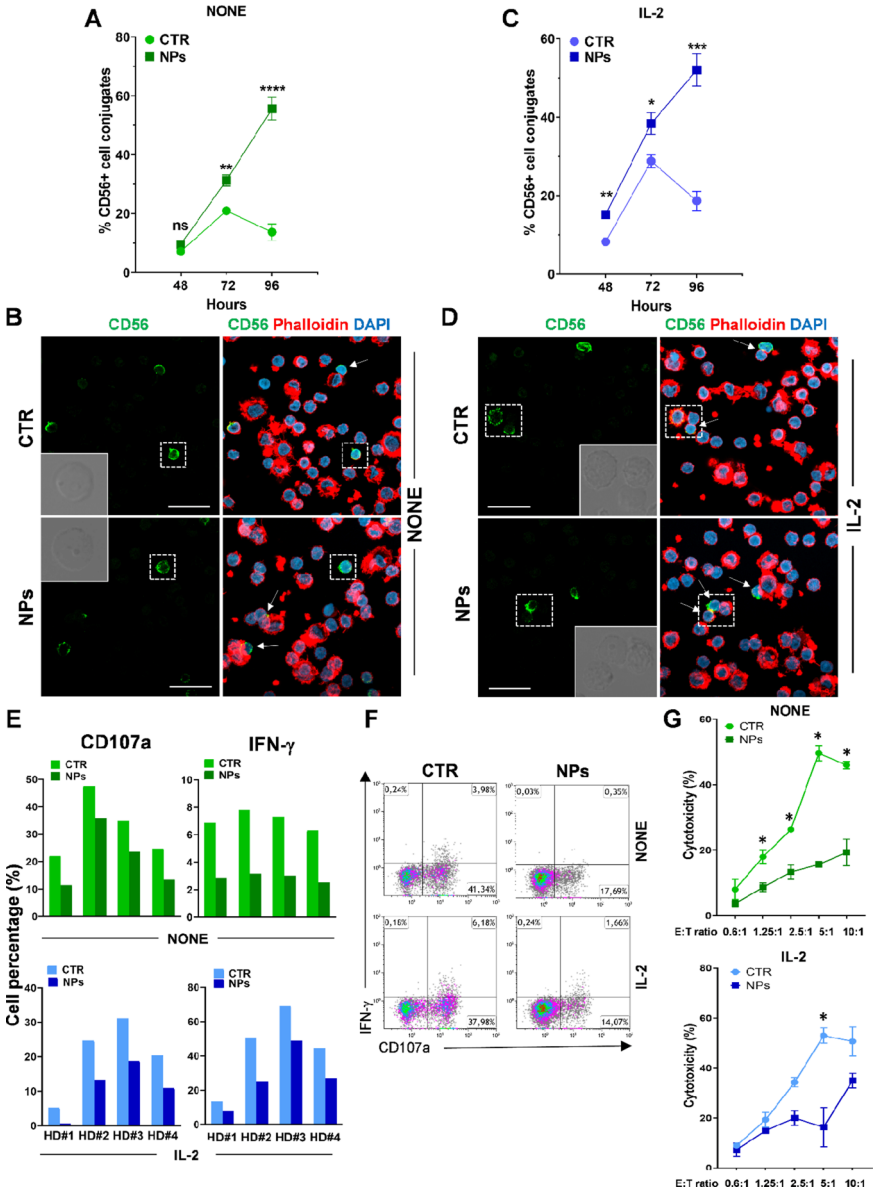

Fig. 4. NPs modulate NK cell interactions and impair cytotoxic function. (**A**, **C**) Quantification of CD56⁺ NK cell conjugates in PBMCs cultured with or without NPs under control or IL-2-stimulated conditions over time; $^{*}p \leq 0.05$, $^{**}p \leq 0.01$, $^{***}p \leq 0.001$, $^{****}p \leq 0.0001$. (**B**, **D**) CLSM images showing increased CD56⁺ NK cell interactions (white arrows) in NP-exposed cultures without evident morphological alterations as showed in transmission light image magnified ROI (dotted lines). Scale bars=20 µm. (**E**) NK cell degranulation and cytokine production, assessed by CD107a and IFN-γ following stimulation with K562 target cells in four HDs. (**F**) Representative flow cytometry plots of NK activity, measured by CD107a expression and IFN-γ production. (**G**) NK cell-mediated cytotoxicity against K562 cells at different E: T ratios. Data are representative of three independent experiments or shown as mean ± SE; $^{*}p \leq 0.05$.

integrate these observations with the alterations in lymphocyte phenotype and interactions, we assessed the production of key immune-modulating factors, including chemokines, cytokines, soluble immune receptors, metalloproteinases, growth factors, and transcription factors in PBMCs, with or without IL-2. The analysis was conducted either at the transcriptional level following 48 h and 96 h exposure to NPs and at the protein level in the supernatants of cultures at 96 h. Unsupervised clustering of transcriptome data showed that NPs induced time-dependent immunosuppressive effects, stronger in naïve PBMCs than with IL-2. After 48 h-NP exposure, PBMCs displayed downregulation of IL-12, IL-21, IL-4, IL-15, PD-1, and transcription factors IRF-4, Blimp-1 (PRDM1) and IRF-8, alongside upregulation of CXCL8 and IL-10. By 96 h, the transcriptome showed a pronounced immunosuppressive profile, with strong downregulation of pro-inflammatory molecules (IL-6, CXCL8, IL-1β, TNF, IFN-γ, IL-12, IL-21) while IRF-4 remained suppressed, and IL-10 was markedly upregulated, indicating a shift toward a tolerogenic environment potentially dampening both innate and adaptive responses (Fig. 6B). Proteomic analysis confirmed the transcriptomic results. After 96 h-NP exposure, PBMCs

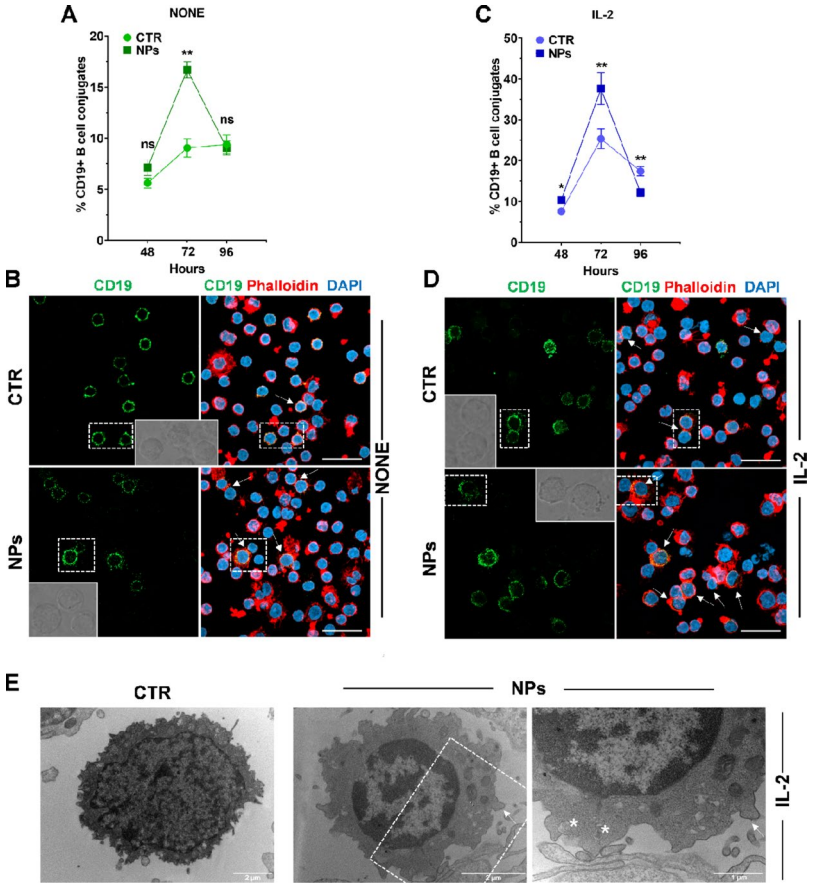

Fig. 5. NPs alter CD19⁺ B lymphocyte interactions and ultrastructure. (**A**, **C**) Time-course quantification of CD19⁺ B-cell conjugates in PBMCs cultured with or without NPs under control or IL-2-stimulated conditions. Data are mean% ±SE; $^{*}p \leq 0.05$, $^{**}p \leq 0.01$. (**B**, **D**) CLSM images of PBMCs ± NPs showing increased CD19⁺ B-cell interactions (white arrows). mainly in IL-2-stimulated cultures. Transmission light image insets highlight intracellular vesicles in NP-exposed cells. Scale bars = 20 µm. (**E**) TEM analysis of IL-2-stimulated CD19⁺ B cells ± NPs showing altered cytoplasmic organization and vesicle accumulation; white arrows indicate CD19 immunogold labelling; the right panel shows a magnified ROI and asterisks indicate vacuoles with NP-like structures. All data are representative of three independent experiments.

showed downregulation of TNF, IL-6, IL-17, CD163, TIMP1, and CXCL1, with IL-2-stimulated PBMCs also showing reduced MMP10, CCL3, CCL4, and FABP4, indicating suppressed inflammatory responses (Fig. 6C). PCA further revealed that NP exposure dominated over culture conditions, as NP-exposed PBMCs clustered separately from controls regardless of IL-2 treatment (Fig. 6D). As some NP-modulated molecules are myeloid-associated, CD14⁺ monocytes were confirmed to internalize NPs, displaying modest PD-L1 upregulation and reduced HLA-DR compared with controls (Fig. S7).

Exposure to NPs hampers the ability of NK and CD8 + T cells to generate an effective antitumor response

Given the functional immune changes, we assessed the impact of NP exposure on T cell and NK cell anti-tumor activity, using DC/PBL co-cultures to measure the antigen-specific T cell responses. A significant reduction in CD4 + T cells was observed, along with a pronounced downregulation of the activation markers CD69, CD25, and CD38 (Fig. 7A). In addition, although the frequency of memory CD4 + T cells remained stable, there was a notable decrease in CCR4 + CCR6+ Th2 cells and downregulation of Th17 cells, while Th1 cells were unaffected (Fig. 7B). In contrast, CD8⁺ T cell frequency increased, but fully activated cytotoxic subsets (CD8⁺CD69⁺CD137⁺, CD8⁺CD69⁺CD25⁺, CD8⁺HLA-DR⁺CD38⁺) and partially activated CD8⁺HLA-DR⁻CD38⁺ cells were markedly downregulated (Fig. 7C). NP exposure also reduced degranulating CD107a⁺IFN-γ⁺ CD8⁺ T cells (Fig. 7D, E) and significantly impaired their cytotoxic activity against HLA-A2⁺ Karpas-422 lymphoma target cells in the Calcein-AM assay (Fig. 7G). These effects were observed in the context of antigen-driven responses generated in autologous IFN-DC/PBL co-cultures, in which tumor lysate-loaded IFN-DCs were used to prime and expand tumor-reactive effector lymphocytes. Strikingly, NP exposure also compromised NK cytotoxicity immunity within the same antigen-priming co-cultures reducing the frequency of CD3⁻CD56⁺ NK cells co-expressing IFN-γ and CD107a with a marked decrease in NK cell-mediated lysis of K562 target cells in the Calcein-AM assay (Fig. 7D, F, H). Together, these findings demonstrate that NP exposure broadly suppresses both antigen-

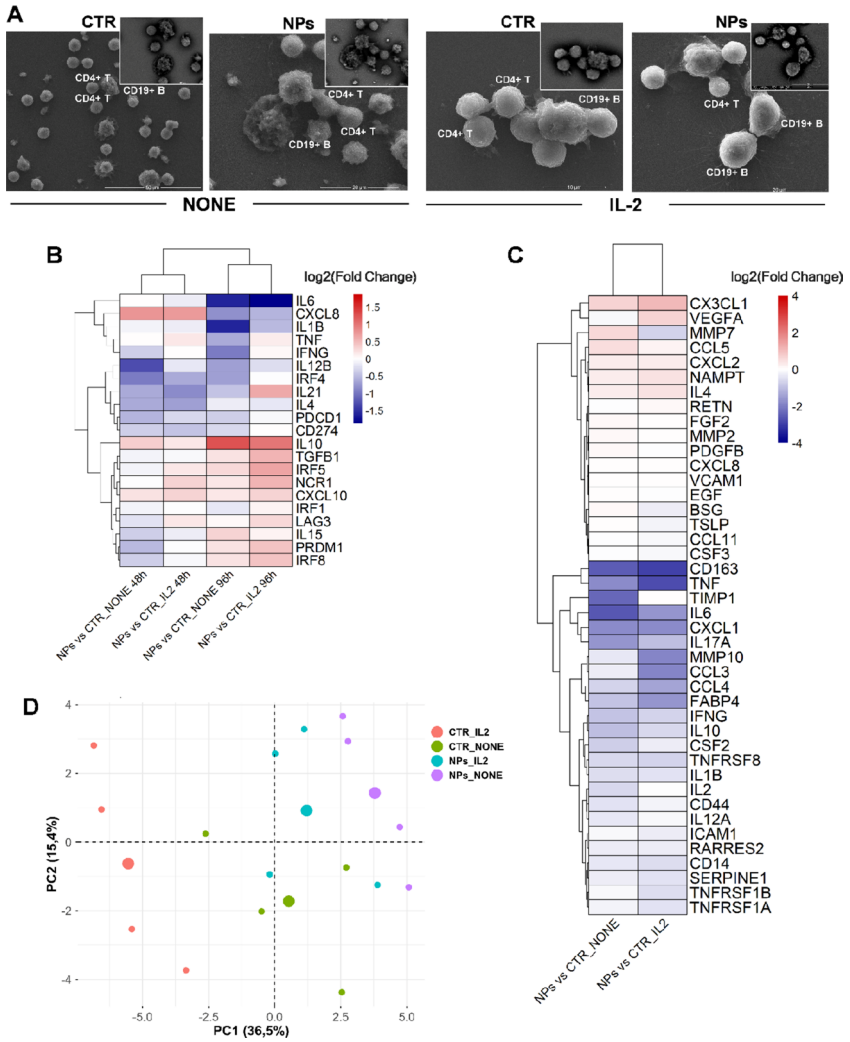

Fig. 6. NPs modulate immune cell interactions and molecular profiles in PBMCs. **(A)** SEM immunolocalization of PBMCs labeled for CD4, CD19, and CD14, showing increased cell interactions after NP exposure and IL-2 stimulation. Images are shown with BSE insets. (**B-C**) Heatmaps of differentially expressed genes (48 h, 96 h) and proteins (96 h) in PBMCs exposed to NPs versus controls. (**D**) PCA of immune-related protein expression in PBMCs cultured for 96 h with or without NPs. Large dots indicate condition means ($n = 4$); small dots represent individual samples. Figures in panels B-D were generated using RStudio software.

specific CD8⁺ T cell responses and NK cell effector functions within a physiologically relevant DC-driven immune activation system, indicating a coordinated impairment of adaptive and innate antitumor immunity.

NPs impair B cell capability in generating antibodies against SARS-CoV-2

To evaluate how NP exposure affects B cell function, we examined SARS-CoV-2-specific memory B cells in PBMCs from vaccinated individuals. NP exposure increased B cell conjugate formation, reaching levels similar to Spike antigen stimulation, and combined NP plus Spike exposure further enhanced cell interactions (Fig. 8A). We then assessed the recall antibody response to Spike antigen. NP exposure alone did not affect IgG in CD19⁺ B cells, which increased with Spike or HA stimulation. However, combined NP and Spike exposure prevented the IgG increase, indicating an inhibitory effect of NPs on antibody production (Fig. 8B, C). Ultrastructural analysis showed that HA or Spike antigens induced plasmacytoid features in CD19⁺ B cells, including irregular nuclei, cytoplasmic extensions, and abundant ER and Golgi, which were substantially diminished after NP exposure (Fig. 8D).

Discussion

Chronic exposure to NPs promotes their internalization by human cells, potentially inducing pathological responses such as cytotoxicity, oxidative stress, and inflammation, and is associated with adverse outcomes including reproductive and cardiovascular effects[7,21]. Although numerous studies in murine models and human cell lines have shown the detrimental biological effects of NPs, including on the immune system, their impact on the function of primary human cells remains poorly explored[22,23]. To date, there is no evidence regarding

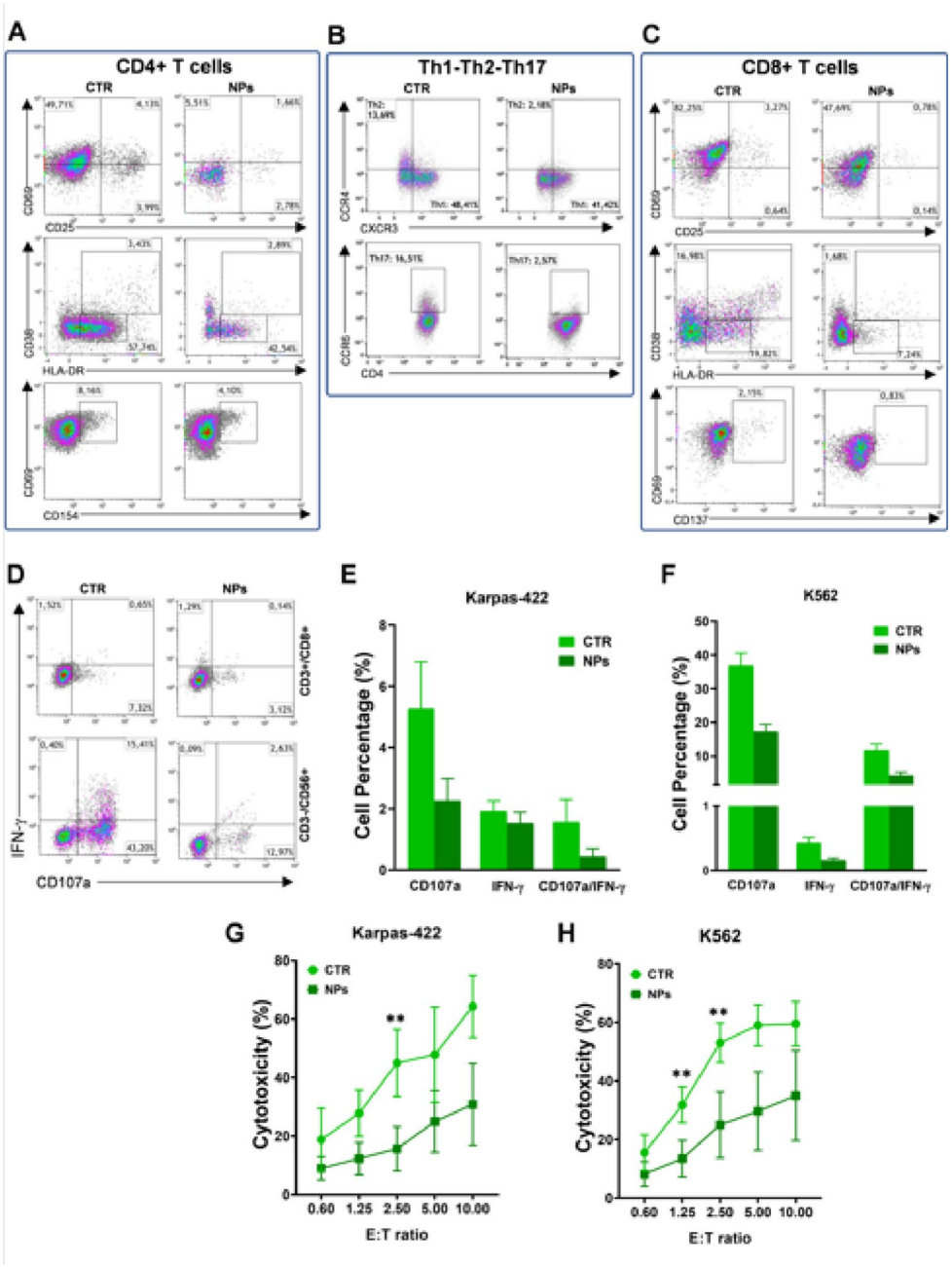

Fig. 7. NPs impair CD8⁺ T cell and NK cell effector functions induced by tumor Ag-loaded IFN-DCs. Phenotypic and functional analysis of PBLs stimulated with tumor lysate-loaded IFN-DCs, in the presence or absence of NPs. (**A**) Activation markers on CD4⁺ T cells. (**B**) Flow cytometric analysis of Th1, Th2, and Th17 CD4⁺ T-cell subsets. (**C**) Activation profiles of CD8⁺ T cells. (**D**) Degranulation and IFN-γ production in CD8⁺ T cells and NK cells. Data in panels A-D are representative of three independent experiments. (**E**) Mean percentages from three independent experiments of CD107a⁺, IFN-γ⁺ and CD107a⁺IFN-γ⁺ CD8⁺ T cells, assessed against Karpas-422. Given three replicates, statistical analysis was performed using a Wilcoxon test on paired measurements across the three experimental blocks, with $p < 0.01$. (**F**) Mean percentages from three independent experiments of CD107a⁺, IFN-γ⁺ and CD107a⁺IFN-γ⁺ NK cells, assessed against K562; statistical analysis was performed using a Wilcoxon test on paired measurements across the three experimental blocks, with $^{**}p \leq 0.01$. (**G**) Ag-specific cytotoxicity of CD8⁺ T cells against Karpas-422 targets. (**H**) NK-cell-mediated cytotoxicity against K562 target cells at different E: T ratios. Data are representative of three independent experiments. Statistical significance was assessed by Wilcoxon test, $^{**}p \leq 0.01$.

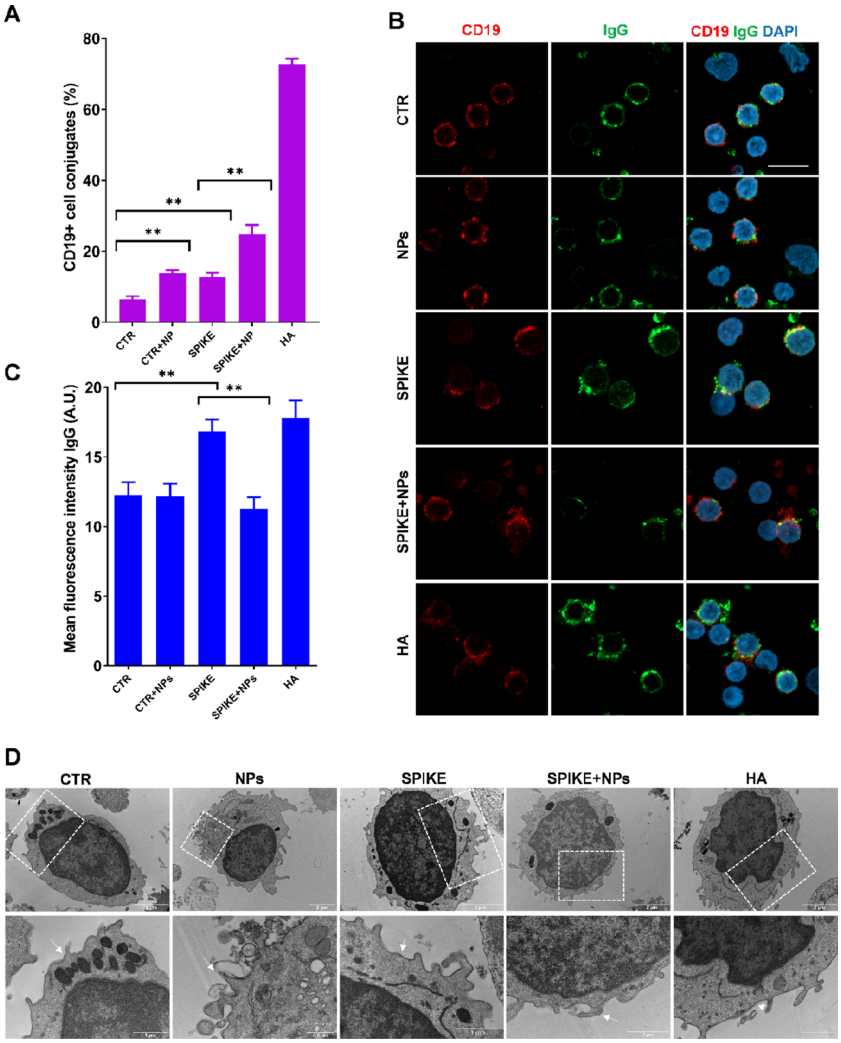

Fig. 8. Effects of NPs on IgG production in B lymphocytes in response to Spike antigen. (**A**) Frequency of CD19⁺ B-cell conjugates in PBMC cultures from SARS-CoV-2-vaccinated donors, stimulated with Spike or left unstimulated (CTR), with or without NP exposure for 72 h. HA stimulation served as a positive control. Data are mean %±SE; $^{**}p \leq 0.01$. (**B**) Representative CLSM images of CD19⁺ B cells from CTR or Spike-stimulated PBMCs ± NPs, stained for CD19 (red), IgG (green), and nuclei (blue). NP exposure reduces surface IgG in Spike-stimulated cells. Scale bars= 10 µm. (**C**) IgG Mean fluorescence intensity (MFI) in CD19⁺ B cells after Spike stimulation, showing increased IgG that is inhibited by NP exposure. Data are shown as MFI ± SE; $^{**}p \leq 0.01$. (**D**) TEM analysis of CD19⁺ B cells from CTR or Spike-stimulated PBMCs ± NPs. Spike- and HA-stimulated cells display plasmacell-like morphology, whereas NP-exposed Spike-stimulated cells show altered ultrastructural features. Lower panels show magnified regions; white arrows indicate immunogold labeling for IgG. Representative of three independent experiments.

their effects on the functionality of key human immune cells responsible for mediating innate and adaptive immune responses. In this study, we investigated the effects of NPs on human lymphocyte subsets that govern both innate and adaptive immunity, evaluating their impact at both phenotypic and functional levels. Our results demonstrate impaired immune functions, leading to defective responses to tumor and viral antigens and potentially compromising effective antitumor and antiviral immunity.

NPs interact with the immune system through multiple pathways, with peripheral blood representing one of the most critical interfaces[13]. In this study, we first replicated the initial stage of NP entry into the bloodstream, where contact with plasma components leads to the formation of a biocorona, a key determinant of subsequent interactions with immune cells[24]. Notably, ox-NPs, which resemble environmentally aged NPs, exhibited altered physicochemical properties that, upon biocorona acquisition, promoted surface functionalization and resulted in extensive agglomeration[25]. Consistent with previous reports[26], the dynamic changes in size, charge, and polydispersity are likely to critically influence NP-immune cell interactions, emphasizing the importance of using biologically conditioned NPs when assessing their immunological effects. Importantly, this process is not limited to peripheral blood, as NP-exposed immune cells can migrate to other tissues and organs, potentially

affecting their function. We therefore assessed NP effects on major human immune populations, examining both phenotype and function.

As an initial functional assessment, we show that NP exposure markedly enhances interactions across all lymphocyte subsets in PBMCs without cytotoxicity. Notably, for the first time, we demonstrate that NP exposure drives $CD4^+$ T cells toward a deactivated state, downregulating key activation markers and forming NP-containing vacuoles, with IL-2 failing to prevent later suppression of proliferation and interactions, indicating accelerated T cell exhaustion[27]. Similarly, NP exposure modulates human $CD8^+$ T cells by enhancing interactions and forming highly granular clusters by 72 h, while downregulating activated ($CD8^+CD69^+CD25^+$, $CD8^+HLA\text{-}DR^+CD38^+$) and recently activated cytotoxic ($CD8^+CD69^+CD137^+$) subsets. With IL-2, early activation and interactions are preserved but decline over time, accompanied by increased cytoplasmic granularity. Our data align with previous evidence showing that chronic exposure to NPs in mice suppresses $CD8^+$ T-cell differentiation, thereby impairing the development and function of cytotoxic T cells[11]. Of interest, NPs also significantly affect NK cells, with some effects distinct from those observed in T cells. While NP exposure enhanced NK cell interactions, it had limited impact on granularity and did not reduce interactions over time with IL-2. However, NP-exposed NK cells showed marked decreases in degranulating IFN-$\gamma^+CD107a^+$ cells and cytotoxicity against K562 targets, indicating substantial functional impairment. Overall, these results demonstrate that NPs can compromise highly heterogeneous and plastic lymphocyte populations, including $CD4^+$ and $CD8^+$ T cells and NK cells, critical for antitumor effector responses[28]. Accordingly, and most importantly, our study demonstrates for the first time that NP exposure directly compromises antitumor responses driven by tumor cell antigens.

$CD8^+$ T cells stimulated with DCs loaded with cancer cell lysates in the presence of NPs showed a marked reduction in IFN-$\gamma^+CD107a^+$ degranulating populations and a corresponding loss of cytotoxic activity against the same cancer cells, indicating suppression of antitumor T cell function. Similarly, $CD4^+$ T cells from these cultures exhibited downregulation of activated subsets ($CD4^+CD69^+CD25^+$, $CD4^+CD38^+HLA\text{-}DR^+$, $CD4^+CD69^+CD154^+$), mild suppression of Th1 and Th17, and pronounced inhibition of Th2 cells. NK cell activity was also impaired, with fewer IFN-$\gamma^+CD107a^+$ degranulating cells and reduced lysis of K562 targets. Together, these findings reveal that NPs disrupt functional antitumor responses mediated by both T and NK cells, which are critical for tumor control and the efficacy of immune-based therapies. Moreover, our study reveals that NP exposure directly affects human peripheral B cells. Although survival remained unchanged, NPs increased B cell interactions and triggered notable morphological changes, including cellular enlargement, intracellular granules and NP-containing vacuoles, indicating active uptake. Remarkably, in SARS-CoV-2-vaccinated individuals, NP-exposed B cells exhibited impaired function, with reduced Spike-specific IgG production and loss of plasmacytoid features such as irregular nuclei, cytoplasmic extensions and expanded ER and Golgi[29], revealing NP potential to disrupt antibody production. We hypothesize that NP exposure disrupts Spike antigen-driven B-cell activation and differentiation into antibody-secreting cells. This impairment may involve reduced reprogramming of B cells and defective biogenesis of secretory organelles such as the endoplasmic reticulum and Golgi apparatus, which are required for high-level IgG production[30]. Consequently, NP exposure may lead to incomplete plasma cell maturation and decreased Spike-specific IgG output despite antigen exposure, ultimately weakening the humoral immune response. These findings are particularly relevant in view of the highly efficient and multilayered immune evasion strategies employed by SARS-CoV-2, which promote immune dysregulation and delayed adaptive responses through key mechanisms such as antagonizing IFN-I signaling, impairing innate immune sensing and modulating antigen presentation pathways[31,32]. Crucially, multiple SARS-CoV-2 proteins disrupt host immune regulation, with recent evidence that the original Wuhan strain and its spike protein activate the hypoxia-inducible factor 1 (HIF-1) transcriptional complex in infected cells, leading to suppression of both helper and cytotoxic T-cell functions and potentially fostering pro-tumorigenic processes in affected tissues[33]. Within this framework of viral immune escape, robust B-cell activation is crucial for protective immunity, as conserved spike epitopes have been shown to elicit potent antibodies that neutralize multiple SARS-CoV-2 variants by destabilizing the virus, thereby providing a basis for broadly effective vaccines and therapies[34]. Our data suggest that NP exposure may further disrupt the finely SARS-CoV-2-tuned immune environment by directly impairing B-cell functional reprogramming upon antigen encounter. The observed reduction in Spike-specific IgG production, together with the loss of secretory plasmacytoid morphology following NP exposure, indicates an incomplete antibody-secreting differentiation program, thereby amplifying immune evasion. In line with the functional impairment of T, B, and NK cells, our study also demonstrates that NP exposure profoundly reshapes the cytokine milieu at both transcriptional and protein levels, establishing a markedly immunosuppressive environment[35]. NP exposure drives a pronounced cytokine shift, characterized mainly by suppression of IL-6, TNF-α, IL-17, IL-1β, and IFN-γ, thereby promoting an immunosuppressive Th2-skewed environment that dampens the activation of key effector populations[36]. This coordinated downregulation impairs $CD8^+$ T-cell cytotoxicity and memory formation, reduces Th1/Th17 responses and B-cell help from $CD4^+$ T cells, diminishes B-cell antibody production and plasmablast differentiation, and weakens NK-cell cytotoxicity and cytokine secretion. Taken together, NP exposure induces transcriptional, phenotypic, and functional alterations across multiple human immune cell populations in peripheral blood, consistent with the establishment of a markedly immunosuppressive environment in PBMCs that may compromise effective antitumor and antiviral immune responses.

Materials and methods

NP preparation

or-NPs (100 nm, PolySciences) were subjected to controlled thermal oxidation by treatment at 80 ◦C for 2 h to obtain ox-NPs. This treatment introduces oxygen-containing functional groups on the particle surface, mimicking chemical transformations occurring during environmental weathering, including UV-driven photooxidation and thermo-oxidative aging. In this research, ox-NPs are used as a simplified proxy of environmentally aged NPs,

capturing the critical role of surface oxidation in modulating biological interactions. Ox-NPs were subdivided into aliquots, stored at 4 °C until use[37]. Before incubation with PBMCs, ox-NPs were pre-incubated for 2 h with plasma from the same donor from whom PBMCs were to produce Pl-ox-NPs[38]. This step enables protein corona (biocorona) formation via adsorption of plasma proteins onto NP surfaces. Oxidation enhances protein binding, leading to altered physicochemical properties, including increased hydrophilicity, modified surface charge, and a higher tendency to agglomerate[25]. Autologous plasma was used to preserve donor-specific protein composition, and Pl-ox-NPs were used without further purification to maintain the dynamic corona.

NP measurements

NP morphology was analyzed by TEM after deposition of or-NP and ox-NP suspensions in PBS, as well as Pl-ox-NPs, onto carbon-coated 400-mesh grids, followed by negative staining with 1% phosphotungstic acid and air-drying. Hydrodynamic diameter (Z-average), size distribution, and PDI were determined by DLS using a Zetasizer Ultra instrument (Malvern Instruments). Zeta potential of or-NPs, ox-NPs, and Pl-ox-NPs (100 µg/mL) was measured using electrophoretic light scattering. All measurements were performed in triplicate. Details are detailed in the Supplementary Methods.

Cell preparation and culture with NPs

PBMCs were obtained from buffy coats of healthy donors (HDs), as anonymously provided by the Immunohematology and Transfusion Center of Policlinico Umberto I, University "La Sapienza," Rome, Italy. Informed consent was obtained from blood donors in accordance with the Declaration of Helsinki, and both the informed consent form and procedure were approved by the Ethics Committee of Policlinico Umberto I. All methods were performed in accordance with the relevant guidelines and regulations for human experimentation, and all procedures complied with the ethical standards of the responsible institutional committee. PBMCs were purified as described[39]. Pl-ox-NPs were added at the concentration of 100 µg/ml to PBMCs cultured in RPMI-1640 medium for 4 days, with or without the addition of IL-2 (50U/ml, Roche).

DC/PBL co-cultures for antitumor immune response assays and PBMC cultures for IgG production

The assay to evaluate CD8 + T cell- and NK-driven antitumor responses was established by co-culturing tumor antigen-loaded DCs, specifically IFN-DCs, with autologous PBLs. HLA-A2 expression was assessed in donor samples by flow cytometry using anti-HLA-A2-specific monoclonal antibodies (BD Biosciences). The human B-cell non-Hodgkin lymphoma Karpas-422 cells (Interlab Cell Line Collection) were cultured in RPMI-1640 medium (Gibco) supplemented with 20% fetal bovine serum (FBS), 2 mM L-glutamine, 100 U/mL penicillin, and 100 µg/mL streptomycin. HLA-A2 expression on Karpas-422 cells was evaluated by flow cytometry using anti-HLA-A2 monoclonal antibodies (BD Biosciences). For DC generation, $CD14^+$ monocytes were isolated by immunomagnetic selection (MACS Cell Isolation Kits; Miltenyi Biotec) and cultured at 2×10^6 cells/mL in CellGro DC medium (CellGenix), supplemented with 500 U/mL GM-CSF (Genzyme) and 10,000 U/mL IFN-α2b (Intron A; Schering-Plough) for 3 days. IFN-DCs were pulsed with Karpas-422 tumor cell lysate, obtained as previously reported[40], at a 1:2 ratio for 16 h at 37 °C and subsequently co-cultured with autologous PBLs at a 1:4 ratio. Culture medium was supplemented with recombinant human IL-2 (50 U/mL; Roche) starting on day 3 of co-culture and replenished every 3 days. On day 7, PBLs were restimulated with frozen aliquots of lysate-loaded DCs and effector cells were analyzed 7 days later. For the evaluation of NP effects on Spike-driven IgG production, PBMCs obtained from SARS-CoV-2–vaccinated donors were plated at a concentration of 2×10^6 cells/mL in CellGro medium (CellGenix, USA). Cells were stimulated with recombinant SARS-CoV-2 Spike-Trimer protein from the original Wuhan-Hu-1 strain (5 µg/mL; Miltenyi Biotec) and tetravalent hemagglutinin proteins (HA; influenza A strains HA-H1N1/ H3N2, influenza B strains HA-Victoria/Yamagata; 1 µg/mL; Seqiris) cultured for 5–7 days at 37 °C in 5% CO_2, subsequently collected and processed for immunostaining prior to CLSM, SEM and TEM analyses.

Confocal laser scanning microscopy (CLSM)

PBMCs were seeded on poly-L-lysine-coated glass slides after different time points of culture with or without NPs. For phenotyping, cells were blocked with FcR and stained with antibodies against CD4, CD8, CD19, or CD56, followed by secondary antibodies or streptavidin-Alexa Fluor as needed. Cells were then paraformaldehyde fixed, Triton X-100 permeabilized, and stained with phalloidin and DAPI for actin and nuclei. IgG in B cells was detected with Alexa Fluor-488 goat anti-human IgG after fixation and permeabilization. CLSM was performed on a Zeiss LSM980 and images were acquired and processed with Zen 3.3 and Adobe Photoshop. Cell conjugates were quantified as CD-positive with actin clustering/total CD-positive ×100. MFI of cell-specific fluorescent signals, including IgG, was measured using ImageJ.

Immunolabeling SEM and TEM

For SEM, PBMCs were seeded on poly-L-lysine-coated slides, stained with antibodies against CD4 or CD19, followed by secondary antibodies conjugated to gold particles, fixed with glutaraldehyde, OsO_4 post-fixed, dehydrated through ethanol and HMDS, dried, carbon-coated, and imaged using backscattered (BSE) and secondary electrons on a Quanta Inspect F (FEI)[41]. For TEM, PBMCs were labeled with CD4 or CD19 antibodies and gold-conjugated secondary antibodies, fixed with glutaraldehyde, paraformaldehyde and $CaCl_2$ in cacodylate buffer, OsO_4 post-fixed, treated with tannic acid and UA-Zero EM stain, dehydrated, embedded in Agar 100, and ultrathin sections were imaged using a FEI/Philips EM 208 S TEM[42].

Flow cytometry
Cells were stained with fluorochrome-conjugated mAbs specific for the T cell and monocyte markers (HLA-DR, CD38, CD3, CD4, CD8, CD25, CD69, PD-1, CD154, CD14, PD-L1, CD45RA, CCR7, CXCR3, CCR4, CCR6). Cell acquisition and analysis were performed using a Gallios flow cytometer, with electronic gating on $CD3^+CD4^+$ or $CD3^+CD8^+$ T cells and $CD14^+$ monocytes to analyse the expression of activation or inhibitory membrane markers.

Apoptosis assay
Lymphocyte apoptosis following exposure to NPs, with or without IL-2, was assessed by multiparametric flow cytometry after immunophenotyping for CD3, CD4, CD8, CD19 and CD56, using Annexin V(AnnV)/propidium iodide (PI) staining, with data acquired on a Cytoflex LX cytometer and analysed using CytExpert software.

Degranulation assay
PBL degranulation was assessed by co-culture with K562 or Karpas-422 cells, with NK and T lymphocytes identified by CD3 and CD56 staining. Flow cytometric analysis was performed to assess CD107a surface expression and intracellular IFN-γ in $CD3^-CD56^+$ or $CD3^+CD56^-$ cells.

Cytotoxicity assay
Cytotoxic activity against K562 and Karpas-422 cells was measured using a Calcein-AM release assay, with labeled target cells co-cultured with effector cells at varying effector-to-target (10^4 cells)-ratios (E: T, 0.60:1, 1.25:1, 2.50:1, 5.00:1, 10.00:1). Fluorescence was measured to calculate percent specific lysis, which is reported as mean ± SE.

Realtime qRT-PCR
Total RNA was extracted from cells using the Total RNA Purification PLUS Kit (NORGEN Biotek Corp.) and reverse transcribed as described[43]. qRT-PCR was performed in duplicate by using SensiFAST™SYBR® (Bioline) and LightCycler® 480 System (Roche Diagnostics). Values were normalized respect to HPRT gene. Sequences of primers used for qPCR are reported in Table S1.

Multiplex immunoassay analysis
Forty-five immune factors were quantified in culture supernatants using Bio-Plex multiplex assays on a Luminex platform, combining three Human Luminex panels (LXSAHM-10, LXSAHM-15, and LXSAHM-20). Samples were incubated with antibody-conjugated magnetic beads and detected with biotinylated antibodies and fluorescent reporters, with acquisition performed on a Bio-Plex X200 reader using Bio-Plex Manager Software 6.1. Results were expressed as pg/mL, with samples analyzed in replicate, and data are reported as mean ± SD.

Analysis of protein/gene expression
The data obtained from the protein assay and qRT-PCR for the selected proteins and genes, respectively, were pre-processed for statistical analysis using RStudio 2024.04.2 + 764 (Posit Team, 2024. RStudio: Integrated Development Environment for R. Posit Software, PBC, Boston, MA. URL: http://www.posit.co/). Fold Change (FC) for the comparisons of interest were computed using the 'dplyr' package. For protein data, the mean of two experimental replicates for each donor was calculated before further analysis. Log2-transformed FC (Log2FC) values were visualized as heatmaps using the 'pheatmap' package. Raw data from qRT-PCR and Bio-Plex assays were arranged into matrices with immune factors as columns and experimental conditions as rows. PCA was performed in R (v4.4.1) using the prcomp() function, and results were visualized with factoextra biplots of conditions and immune factors.

Statistical analysis
Statistical analyses were performed by Wilcoxon signed-rank test unless otherwise indicated. Differences were considered statistically significant at $p \leq 0.05$(*), $p \leq 0.01$(**), $p \leq 0.001$(***), $p \leq 0.0001$(****). All experiments were performed in at least three independent biological replicates, unless otherwise specified in the figure legends. Data are presented as mean ± standard error (SE). Where applicable, details of the specific statistical tests used for individual datasets are indicated in the corresponding figure legends.

Data availability
The datasets generated and analyzed during the current study are available from the corresponding author upon request.

Received: 26 January 2026; Accepted: 27 April 2026
Published online: 18 May 2026

References
1. De Boever, S., Devisscher, L. & Vinken, M. Unraveling the micro- and nanoplastic predicament: A human-centric insight. *Sci. Total Environ.* **916**, 170262. https://doi.org/10.1016/j.scitotenv.2024.170262 (2024).
2. Ali, N. et al. The potential impacts of micro-and-nano plastics on various organ systems in humans. *EBioMedicine* **99**, 104901. https://doi.org/10.1016/j.ebiom.2023.104901 (2024).
3. Krause, S. et al. The potential of micro- and nanoplastics to exacerbate the health impacts and global burden of non-communicable diseases. *Cell. Rep. Med.* **5**, 101581. https://doi.org/10.1016/j.xcrm.2024.101581 (2024).

4. Du, T. et al. Aging of Nanoplastics Significantly Affects Protein Corona Composition Thus Enhancing Macrophage Uptake. *Environ. Sci. Technol.* **57**, 3206–3217. https://doi.org/10.1021/acs.est.2c05772 (2023).
5. Leslie, H. A. et al. Discovery and quantification of plastic particle pollution in human blood. *Environ. Int.* **163**, 107199. https://doi.org/10.1016/j.envint.2022.107199 (2022).
6. Nijenhuis, W. et al. Improved multivariate quantification of plastic particles in human blood using non-targeted pyrolysis GC-MS. *J. Hazard. Mater.* **489**, 137584. https://doi.org/10.1016/j.jhazmat.2025.137584 (2025).
7. Lamoree, M. H. et al. Health impacts of microplastic and nanoplastic exposure. *Nat. Med.* **31**, 2873–2887. https://doi.org/10.1038/s41591-025-03902-5 (2025).
8. Kim, E. H. et al. Polystyrene nanoplastics promote the blood-brain barrier dysfunction through autophagy pathway and excessive erythrophagocytosis. *Ecotoxicol. Environ. Saf.* **289**, 117471. https://doi.org/10.1016/j.ecoenv.2024.117471 (2025).
9. Tian, S., Li, R., Li, J. & Zou, J. Polystyrene nanoplastics promote colitis-associated cancer by disrupting lipid metabolism and inducing DNA damage. *Environ. Int.* **195**, 109258. https://doi.org/10.1016/j.envint.2025.109258 (2025).
10. Dan, K. B., Yoo, J. Y. & Min, H. The Emerging Threat of Micro- and Nanoplastics on the Maturation and Activity of Immune Cells. *Biomol. Ther. (Seoul).* **33**, 95–105. https://doi.org/10.4062/biomolther.2024.195 (2025).
11. Li, L. et al. Chronic exposure to polystyrene nanoplastics induces intestinal mechanical and immune barrier dysfunction in mice. *Ecotoxicol. Environ. Saf.* **269**, 115749. https://doi.org/10.1016/j.ecoenv.2023.115749 (2024).
12. Sarma, D. K. et al. The Biological Effects of Polystyrene Nanoplastics on Human Peripheral Blood Lymphocytes. *Nanomaterials (Basel).* **12** https://doi.org/10.3390/nano12101632 (2022).
13. Arribas Arranz, J. et al. Kinetics and toxicity of nanoplastics in ex vivo exposed human whole blood as a model to understand their impact on human health. *Sci. Total Environ.* **948**, 174725. https://doi.org/10.1016/j.scitotenv.2024.174725 (2024).
14. Adler, M. Y. et al. Effect of micro- and nanoplastic particles on human macrophages. *J. Hazard. Mater.* **471**, 134253. https://doi.org/10.1016/j.jhazmat.2024.134253 (2024).
15. Wolff, C. M., Singer, D., Schmidt, A. & Bekeschus, S. Immune and inflammatory responses of human macrophages, dendritic cells, and T-cells in presence of micro- and nanoplastic of different types and sizes. *J. Hazard. Mater.* **459**, 132194. https://doi.org/10.1016/j.jhazmat.2023.132194 (2023).
16. Li, Y. et al. In vitro study on the toxicity of nanoplastics with different charges to murine splenic lymphocytes. *J. Hazard. Mater.* **424**, 127508. https://doi.org/10.1016/j.jhazmat.2021.127508 (2022).
17. Rubio, L., Barguilla, I., Domenech, J., Marcos, R. & Hernandez, A. Biological effects, including oxidative stress and genotoxic damage, of polystyrene nanoparticles in different human hematopoietic cell lines. *J. Hazard. Mater.* **398**, 122900. https://doi.org/10.1016/j.jhazmat.2020.122900 (2020).
18. Chiang, C. C., Yeh, H., Shiu, R. F., Chin, W. C. & Yen, T. H. Impact of microplastics and nanoplastics on liver health: Current understanding and future research directions. *World J. Gastroenterol.* **30**, 1011–1017. https://doi.org/10.3748/wjg.v30.i9.1011 (2024).
19. Zhao, L. et al. Prolonged oral ingestion of microplastics induced inflammation in the liver tissues of C57BL/6J mice through polarization of macrophages and increased infiltration of natural killer cells. *Ecotoxicol. Environ. Saf.* **227**, 112882. https://doi.org/10.1016/j.ecoenv.2021.112882 (2021).
20. Alimi, O. S. et al. Weathering pathways and protocols for environmentally relevant microplastics and nanoplastics: What are we missing? *J. Hazard. Mater.* **423**, 126955. https://doi.org/10.1016/j.jhazmat.2021.126955 (2022).
21. Winiarska, E., Jutel, M. & Zemelka-Wiacek, M. The potential impact of nano- and microplastics on human health: Understanding human health risks. *Environ. Res.* **251**, 118535. https://doi.org/10.1016/j.envres.2024.118535 (2024).
22. Li, H. et al. Immunotoxicity of microplastics in fish. *Fish. Shellfish Immunol.* **150**, 109619. https://doi.org/10.1016/j.fsi.2024.109619 (2024).
23. Yang, W. et al. Impacts of microplastics on immunity. *Front. Toxicol.* **4**, 956885. https://doi.org/10.3389/ftox.2022.956885 (2022).
24. Wu, X. et al. Macrophage cytoskeletal and immune responses to photoaged and gastrointestinal-transformed polylactic acid micro/nanoplastics with protein corona. *J. Hazard. Mater.* **498**, 139807. https://doi.org/10.1016/j.jhazmat.2025.139807 (2025).
25. Arredondo-Navarro, A. et al. Thermal oxidation, ultraviolet radiation, and mechanical abrasion - understanding mechanisms of microplastic generation and chemical transformation. *Microplast nanoplast.* **6** https://doi.org/10.1186/s43591-026-00178-5 (2026).
26. Cai, R. et al. Protein Corona-Directed Cellular Recognition and Uptake of Polyethylene Nanoplastics by Macrophages. *Environ. Sci. Technol.* **58**, 14158–14168. https://doi.org/10.1021/acs.est.4c05215 (2024).
27. Miggelbrink, A. M. et al. CD4 T-Cell Exhaustion: Does It Exist and What Are Its Roles in Cancer? *Clin. Cancer Res.* **27**, 5742–5752. https://doi.org/10.1158/1078-0432.CCR-21-0206 (2021).
28. Peng, S. et al. CTLs heterogeneity and plasticity: implications for cancer immunotherapy. *Mol. Cancer.* **23**, 58. https://doi.org/10.1186/s12943-024-01972-6 (2024).
29. Bonaud, A., Khamyath, M. & Espeli, M. The cellular biology of plasma cells: Unmet challenges and opportunities. *Immunol. Lett.* **254**, 6–12. https://doi.org/10.1016/j.imlet.2023.01.005 (2023).
30. Di Conza, G., Ho, P. C., Cubillos-Ruiz, J. R. & Huang, S. C. Control of immune cell function by the unfolded protein response. *Nat. Rev. Immunol.* **23**, 546–562. https://doi.org/10.1038/s41577-023-00838-0 (2023).
31. Sievers, B. L., Cheng, M. T. K., Csiba, K., Meng, B. & Gupta, R. K. SARS-CoV-2 and innate immunity: the good, the bad, and the goldilocks. *Cell. Mol. Immunol.* **21**, 171–183. https://doi.org/10.1038/s41423-023-01104-y (2024).
32. Minkoff, J. M. & tenOever, B. Innate immune evasion strategies of SARS-CoV-2. *Nat. Rev. Microbiol.* **21**, 178–194. https://doi.org/10.1038/s41579-022-00839-1 (2023).
33. Abooali, M. et al. Wuhan strain of SARS-CoV-2 triggers activation of immune evasion machinery similar to the one operated by cancer cells. *Front. Immunol.* **16**, 1599352. https://doi.org/10.3389/fimmu.2025.1599352 (2025).
34. Harit, A. et al. Monoclonal antibodies from COVID-19 convalescent patients target cryptic epitopes for broad SARS-CoV-2 neutralization. *Proc. Natl. Acad. Sci. U S A.* **123**, e2523864123. https://doi.org/10.1073/pnas.2523864123 (2026).
35. Pradhan, R., Kundu, A. & Kundu, C. N. The cytokines in tumor microenvironment: from cancer initiation-elongation-progression to metastatic outgrowth. *Crit. Rev. Oncol. Hematol.* **196**, 104311. https://doi.org/10.1016/j.critrevonc.2024.104311 (2024).
36. Hanahan, D., Michielin, O. & Pittet, M. J. Convergent inducers and effectors of T cell paralysis in the tumour microenvironment. *Nat. Rev. Cancer.* **25**, 41–58. https://doi.org/10.1038/s41568-024-00761-z (2025).
37. Mielczarski, J. A., Jeyachandran, Y. L., Mielczarski, E. & Rai, B. Modification of polystyrene surface in aqueous solutions. *J. Colloid Interface Sci.* **362**, 532–539. https://doi.org/10.1016/j.jcis.2011.05.068 (2011).
38. van den Berg, A. E. T. et al. Environmentally weathered polystyrene particles induce phenotypical and functional maturation of human monocyte-derived dendritic cells. *J. Immunotoxicol.* **19**, 125–133. https://doi.org/10.1080/1547691X.2022.2143968 (2022).
39. Lapenta, C. et al. NK Cell Activation in the Antitumor Response Induced by IFN-alpha Dendritic Cells Loaded with Apoptotic Cells from Follicular Lymphoma Patients. *J. Immunol.* **197**, 795–806. https://doi.org/10.4049/jimmunol.1600262 (2016).
40. Lapenta, C. et al. Anti-Tumor Immunity to Patient-Derived Breast Cancer Cells by Vaccination with Interferon-Alpha-Conditioned Dendritic Cells (IFN-DC). *Vaccines (Basel).* **12** https://doi.org/10.3390/vaccines12091058 (2024).
41. Pati, S., Maity, A., Banerji, P. & Majumder, S. B. Qualitative and quantitative differentiation of gases using ZnO thin film gas sensors and pattern recognition analysis. *Analyst* **139**, 1796–1800. https://doi.org/10.1039/c3an02021e (2014).
42. Carpentieri, G. et al. Dominantly acting variants in ATP6V1C1 and ATP6V1B2 cause a multisystem phenotypic spectrum by altering lysosomal and/or autophagosome function. *HGG Adv.* **5**, 100349. https://doi.org/10.1016/j.xhgg.2024.100349 (2024).

43. Fragale, A. et al. Reversing vemurafenib-resistance in primary melanoma cells by combined romidepsin and type I IFN treatment through blocking of tumorigenic signals and induction of immunogenic effects. *Int. J. Cancer*. **153**, 1080–1095. https://doi.org/10.1002/ijc.34602 (2023).

Acknowledgements
The authors acknowledge the FAST facility (ISS, Rome) for providing flow cytometry support.

Author contributions
SM.S. designed the concept, conducted the experiments, analyzed data, and contributed to writing the manuscript. F.S. and A.P. performed the experiments, applied software tools, generated data visualizations, conducted data analyses, and contributed to writing the manuscript. I.C., C.L., A.F., L.L., S.R. and G.R. performed the experimental studies and processed the data. B.B. performed the experiments, processed the data and contributed to writing the manuscript. S.G. performed bioinformatics analysis. M.C., F.F. and C.S. performed the experimental assays. A.F., G.R. and C.S. had a critical scientific revision on the manuscript. L.G. designed the concept, supervised the research, wrote, edit and revised the manuscript, managed project administration. All of the authors read and approved the final manuscript.

Funding
This research was supported by the project grant "ECS00000024 – Rome Technopole Foundation" under the EU-NextGeneration PNRR - Mission 4, Component 2, Investment 1.5 (CUP I83C22001000005)" Rome Technopole – Innovation Ecosystem" - Sub-project: Building solutions for healthcare (Deep-Immune-Host-analysis model).

Declarations

Competing interests
The authors declare no competing interests.

Consent for publication
The manuscript is approved by all authors for publication.

Ethics approval
This work has received approval for research ethics from Istituto Superiore di Sanità Review Board (Istituto Superiore di Sanità, Rome, Italy) and a proof/certificate of approval is available upon request (CE number: AOO-ISS – 21/02/23–0008151 PRE BIO CE 01.00). Written informed consent to participate in this study was provided by the personnel of the Blood Transfusion Service and Hematology Department of Umberto I Hospital (Rome, Italy).

Additional information
Supplementary Information The online version contains supplementary material available at https://doi.org/10.1038/s41598-026-51193-8.

Correspondence and requests for materials should be addressed to L.G.

Reprints and permissions information is available at www.nature.com/reprints.

Publisher's note Springer Nature remains neutral with regard to jurisdictional claims in published maps and institutional affiliations.